Vol. 22, e220006 (2025)
doi: 10.2142/biophysico.bppb-v22.0006

Biophysics and Physicobiology
https://www.jstage.jst.go.jp/browse/biophysico/

*Regular Article*

# Gliding direction of *Mycoplasma mobile* correlates with the curved configuration of its cell shape

Kana Suzuki[1], Daisuke Nakane[2], Masaki Mizutani[1], Takayuki Nishizaka[1]

[1] *Department of Physics, Gakushuin University, Tokyo 171-8588, Japan*
[2] *Department of Engineering Science, Graduate School of Informatics and Engineering, The University of Electro-Communications, Tokyo 182-8585, Japan*

Received January 17, 2025; Accepted February 17, 2025;
Released online in J-STAGE as advance publication February 26, 2025
Edited by Hiroko Bannai

**The gliding motility of bacteria is not linear but somehow exhibits a curved trajectory. This general observation is explained by the helical structure of protein tracks (Nakane et al., 2013) or the asymmetric array of gliding machineries (Morio et al., 2016), but these interpretations have not been directly examined. Here, we introduced a simple assumption: the gliding trajectory of *M. mobile* is guided by the cell shape. To test this idea, the intensity profile of a bacterium, *Mycoplasma mobile*, was analyzed and reconstructed at the single-cell level from images captured under a highly stable dark-field microscope, which minimized the mechanical drift and noise during sequential image recording. The raw image with the size of ~1 μm, which is about four times larger than the diffraction limit of visible light, was successfully fitted by double Gaussians to quantitatively determine the curved configuration of its shape. By comparing the shape and curvature of a gliding motility, we found that the protruded portion of *M. mobile* correlated with, or possibly guided, its gliding direction. Considering the balance between decomposed gliding force and torque as a drag, a simple and general model that explains the curved trajectory of biomolecules under a low Reynolds number is proposed.**

**Key words:** gliding of bacteria, curved trajectory of biomolecule, Gaussian fitting of image, molecular drag, dark-field microscopy

***Significance***

Bacteria move in a variety of ways. Among them, *Mycoplasma mobile* shows flask shape and glides on a solid surface with a curved trajectory. In this study, we captured sequential images of *M. mobile* under an optical microscope, and quantitatively analyzed the shape of every single cell by 2D fitting function in each image. Cell shape was correlated to orientation of curvature, suggesting the front protrusion of the cell guides gliding direction. Finally, we formulate a simple model allowing to explain results. Our new method can be applicable to other bacteria that move with a curved trajectory in different mechanism.

## Introduction

Most bacteria can move unidirectionally. This ability, which was acquired through evolutionary life processes, is required to direct the cell toward a desirable environment for survival [1]. Certain bacteria having a flagellar motor, such as *Escherichia coli* or *Campylobacter jejuni*, exhibit swimming by rotating multiple helical screws [2,3]. *Spiroplasma* can also swim by switching the helicity of its cell shape with a translation of the kink portion that connects different helices [4].

Corresponding author: Takayuki Nishizaka, Department of Physics, Gakushuin University, Tokyo 171-8588, Japan.
ORCID iD: https://orcid.org/0000-0003-2902-3903, e-mail: takayuki.nishizaka@gakushuin.ac.jp

In contrast, a variety of bacteria, such as cyanobacteria, *Flavobacteria*, and *Mycoplasma*, adhere to and displace on a solid surface. Their characteristic trajectories are unique and depend on the type of inherent supramolecular machinery.

Not surprisingly, bacteria with surface motility do not show a uniform motion in a straight line on substrates, even on highly flattened glass. In cyanobacteria, cells show a random wiggling called 'twitching' by using a filamentous structure, pilus. Repeated cycles of extension and retraction of multiple pili induce staggering, which is supported by phototaxis [5]. In *Flavobacterium johnsoniae*, aggregated cells protruding from the colony follow a continuous curved trajectory on an agar plate, which is leftward with few exceptions [6]. The directionality is possibly related to the left-handed helical loop structure around the cell body on which adhesin runs [7].

Notably, in addition to the above examples of random or directed curved gliding, some bacteria show both (rightward- and leftward-curved) trajectories keeping a stable curvature [8,9]. One may think that the directionality depends on a heterogeneous arrangement of motor units. However, all force vectors generated by single motor elements simply merge into only one vector even in the case that the units distribute three-dimensionally around the cell surface. Therefore, the heterogeneity of motor distribution is inadequate in explaining a curved trajectory without large fluctuation. Even when the vector sum tilts against a cell body, the cell should show a straight movement keeping a tilted body against the translation. A general rule describing the curved gliding of bacteria is needed.

In the movement of small objects such as a bacterium in water, inertia is neglected as its Reynolds number is very low [10]. Forces or torques are thus always balanced with molecular drag to keep a constant speed, as in the case of motion generated by motor proteins [11]. The turn mechanism of a man-made car with front and rear wheels simply cannot be applied to the curved trajectory of a bacterium: particularly, drag should be appropriately modeled and formulated to explain trajectories in each species.

To consider the mechanism of circular trajectories of gliding bacteria, we here focused on *Mycoplasma mobile*. This species has a flask-shaped cell of ~1 μm that exhibits the fastest gliding among *Mycoplasma*, with a constant speed of 2.0–4.5 μm $s^{-1}$ in the direction of the cell protrusion [12,13]. *M. mobile* lacks genes encoding conventional surface appendages in bacteria such as flagella and pili [14]. Instead, eight proteins are identified as parts of the gliding machinery: Gli123 [15], Gli521 [16], Gli349 [17], MMOB1660, MMOB1670, MMOB1630, MMOB1620 and MMOB4530 [18] forming a complex including paralogs of F-type ATPase/synthase α and β subunits [19–21]. It was hypothesized that the chemical energy of ATP hydrolysis, occurring at the complex, generates mechanical tilting of a 'leg (Gli349)' protruded from the cell surface through a 'crank (Gli521)', i.e., the rotation of Gli521 driven by motor may be transmitted to a linear motion of the bacterium as a crank, similar to the inverse of a connecting rod and wheels of a man-made steam train [22]. The number of machinery units has been estimated to be ~450, and each of them localizes around the cell neck regularly [12,15]. The unit arrangement is supported by a cytoskeletal array termed 'jellyfish structure' [23]. Morio et al. proposed that the curved gliding trajectory of *M. mobile* results from the difference between the number of right- and left-tilted gliding units [8]. However, as mentioned above, the non-uniformity of the units may affect the tilting angle of the cell body against a gliding line but should not determine the curvature of a whole trajectory.

Here we introduced a simple assumption, that the gliding trajectory of a single bacterium directly links to the configuration of the cell body. To test this, a precise tracking method was first applied to single *M. mobile* cell to acquire curved trajectories. This technique was first developed as an extension of a single-molecule experiments [24] and later generalized to track sub-nanometer- or micron-sized objects by our research group [25–29]. An analysis technique was then developed that enables the quantitative reconstruction of a cell shape from fitting parameters. Fitting was performed within the framework of a conventional data analysis software, and thus one may apply the analysis to any micrometer-sized bacterium. By combining these two methods, we found that the protruded-head portion correlated to, or possibly guided, the gliding direction of *M. mobile*.

## Materials and Methods

### Cultivation of *M. mobile*

A solution containing 2.1% (wt/vol) heart infusion broth, 0.56% (wt/vol) yeast extract, and adjusted pH to 7.8 by NaOH was sterilized with an autoclave. After cooling the solution to room temperature, 10% (vol/vol) horse serum and 50 μg $mL^{-1}$ ampicillin at a final concentration were added to prepare Aluotto medium. A mutant strain of *M. mobile*, P476R *gli521* [30,31], which binds to sialylated oligosaccharides more tightly than the wild-type strain, was used in this study. Cells were cultivated in 10-mL Aluotto medium for 2-3 days at 25 °C in a 25-mL flask without shaking. Cells in a 1-mL culture were collected by centrifugation at 12,000 × *g* for 4 min at 25 °C, resuspended with a micropipette in 200 μL Aluotto medium. The medium was further diluted referring to absorbance at 600 nm to the desired concentration, and subsequently infused into the flow cell for observation [22]. Unbound cells were washed by infusing 60 μL phosphate buffer saline (1.4 mM NaCl, 27 mM KCl, 81 mM $Na_2HPO_4$, 14.7 mM $KH_2PO_4$, and 20 mM glucose) after 5 min. Side edges of coverslips were covered by white petrolatum to avoid evaporation of PBS.

**Microscopy**

*M. mobile* was visualized as a dark-field image under an inverted microscope (TE2000-E) equipped with 100× objective (Plan Fluor 100×/0.5-1.3 Oil; Nikon Instruments), a condenser (Oil 1.43-1.20; Nikon Instruments), a highly-stable customized stage (Chukousha), and an optical table (RS-2000; Newport). Images were recorded by using a high-speed CCD camera system (HDR1600; Digimo). All optical components were enclosed in a thermostatic chamber and operated from the outside of the chamber [32]. In this setup, the position of immobilized *M. mobile* is able to be determined with ±2–4 nm resolution, as a standard deviation from the average value, by 2D Gaussian fitting for 5 s recording with a rate of 30 frames per second.

**Analysis of image**

The images used for analysis were recorded at 30 frames per second with an exposure time of 0.033 s. Note that a gliding cell displaces ~100 nm/frame, as *M. mobile* glides at a speed of 2.0–4.5 μm $s^{-1}$, which is sufficient to capture a raw shape of a single bacterium. The curve-fitting procedure in data analysis software (Igor Pro; WaveMetrics) was applied to either the 8-bit intensity profile of a single bacterium. The software is implemented with a 2D Gaussian as a built-in function, including the cross-correlation term, *cor*, as $I_0 + A \times \exp\{-[((x-x_0)/\sigma_x)^2/2 + ((y-y_0)/\sigma_y)^2/2 - cor(x-x_0)(y-y_0)/\sigma_x\sigma_y]/[2(1-cor^2)]\}$, where $I_0$ is the back-ground intensity; $A$ is the peak intensity of bacterium image; and $\sigma_x$ and $\sigma_y$ are intensity variances along the $X$ and $Y$ axis, respectively. Previously, the center of the image profile of ellipsoidal bacteria was determined as $(x_0, y_0)$ [22]. To acquire an absolute angle of the profile, rotational coordinates were applied instead of *cor*

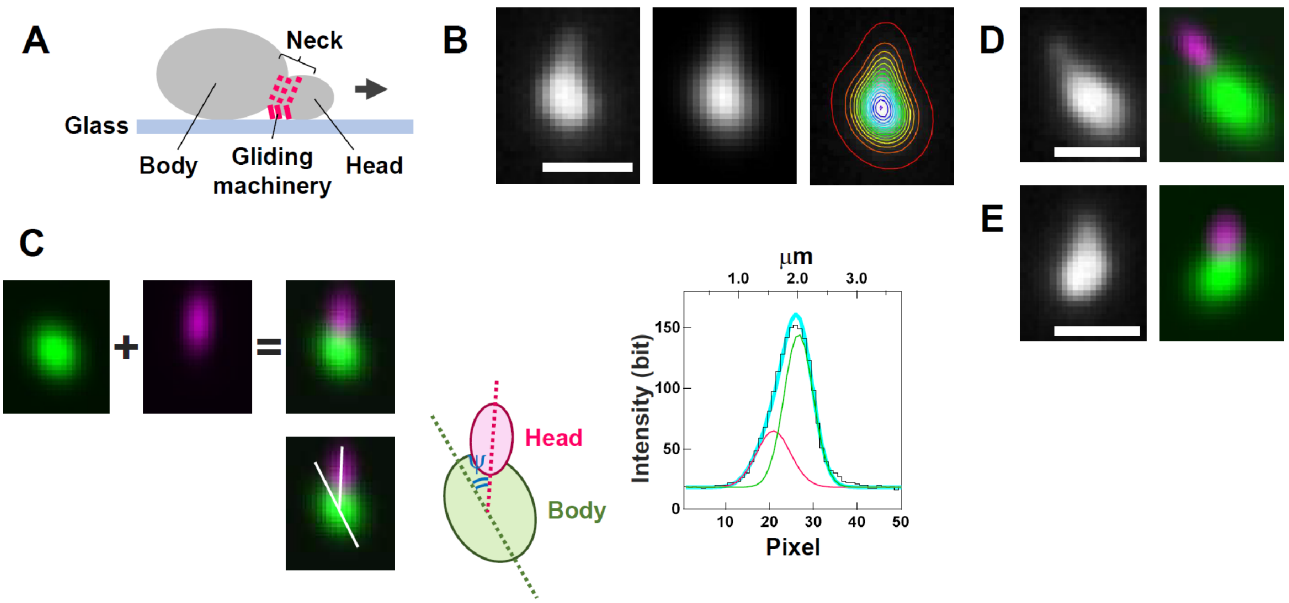


**Figure 1** (A) Schematic diagram of a side view of a *Mycoplasma mobile* cell and its gliding machinery. (B) *Left*, representative dark-field image of a single *M. mobile* cell. The cell gliding on the glass substrate was recorded as a sequential image at 30 frames per second with an exposure time of 0.033 s, typically for 5 s, and one picture was taken and displayed. Scale bar, 1 μm. *Middle*, fitted image to the intensity profile of an original image (*left*) by applying the summation function of double 2D Gaussians. The difference between the two images is hardly recognized as the fitted image was successfully reconstructed with our method. *Right*, contour plot of fitting image merged on the raw image. The red and purple contour lines are 20 and 150, respectively, and the lines between them increase by 10. (C) *Left*, procedure to determine the curved shape of a single cell. Reconstructed image (Figure 1B *Middle* includes 13 parameters. Two sets of six parameters allow us to picture a body part (green) and a head part (magenta), independently, and then the whole image was reconstructed as a merged image. The shape can be determined, in a quantitative manner, as the difference between the angles of the two main axes of the two Gaussians (two white lines in the of merged image and magenta & green dotted lines in the schematic). *Right*, intensity of the raw dark-field image (black) and fitted image (cyan). Cyan curve is the sum of two Gaussians, i.e., one Gaussian for the cell body (green) and the other for the head (magenta). One pixel corresponds to 75 nm. (D, E) Other examples. *Left*, raw images. *Right*, reconstructed images with pseudo-color, in which green and magenta represent body and head, respectively.

in this study. Briefly, we introduced the function $f_{body}$ to depict a body part of *M. mobile* as $f_{body} = A \times \exp\{-[((x - x_a)/\sigma_x)^2/2 + ((y - y_a)/(r_a \times \sigma_x))^2/2]\}$, where $r_a$ is the ratio $\sigma_y/\sigma_x < 1$ to set $\sigma_x$ as the long axis; and $(x_a, y_a) = (((x - x_0) \times \cos\phi - (y - y_0) \times \sin\phi), ((x - x_0) \times \sin\phi + (y - y_0) \times \cos\phi))$ to get the tilting angle $\phi$. Similarly, $f_{head}$ depicts a head part as $f_{head} = A \times r_{int} \times \exp\{-[((x - x_b)/\sigma_x')^2/2 + ((y - y_b)/(r_b \times \sigma_x'))^2/2$, where $r_{int}$ is the ratio of the peak intensity of the head against that of the body; $\sigma_x'$ and $\sigma_y' = r_b \times \sigma_x'$ are intensity variances of the head along the long and short axis, respectively; $(x_b, y_b) = (((x - x_0) \times \cos(\phi + \psi) - (y - y_0) \times \sin(\phi + \psi) - R \times \sigma_x), ((x - x_0) \times \sin(\phi + \psi) + (y - y_0) \times \cos(\phi + \psi)))$ to get both $\psi$, the tilting angle of the head against the body; and $R$, the eccentricity of the center of the head from the body center (normalized by $\sigma_x$) along the long axis. Finally, the equation $f = f_{body} + f_{head} + I_0$ was used for fitting the profile of a sole *M. mobile* cell to reconstruct any flask shape, as both head and body sizes are close to the wavelength of light for observation considering Abbe's diffraction limit.

## Results and Discussion

### Quantification of the shape of a single bacterium cell

*M. mobile* is represented as a flask shape [33], i.e., its cell body has a sharp protrusion at the front that we refer to hereafter as a 'head' (Figure 1A). However, the detailed features of their shape, such as thickness or bending of compartments, have not yet been described because the size of this bacteria is about 1 μm and only about four times larger than the diffraction limit of optical microscopes. To quantify the shape of an asymmetric object with the size of a bacterium, we established a concise method by applying the modified fitting function of a commercial image-analysis platform. In general, the image profile of a single fluorescent emitter can be approximated using the symmetric 2D Gaussian function

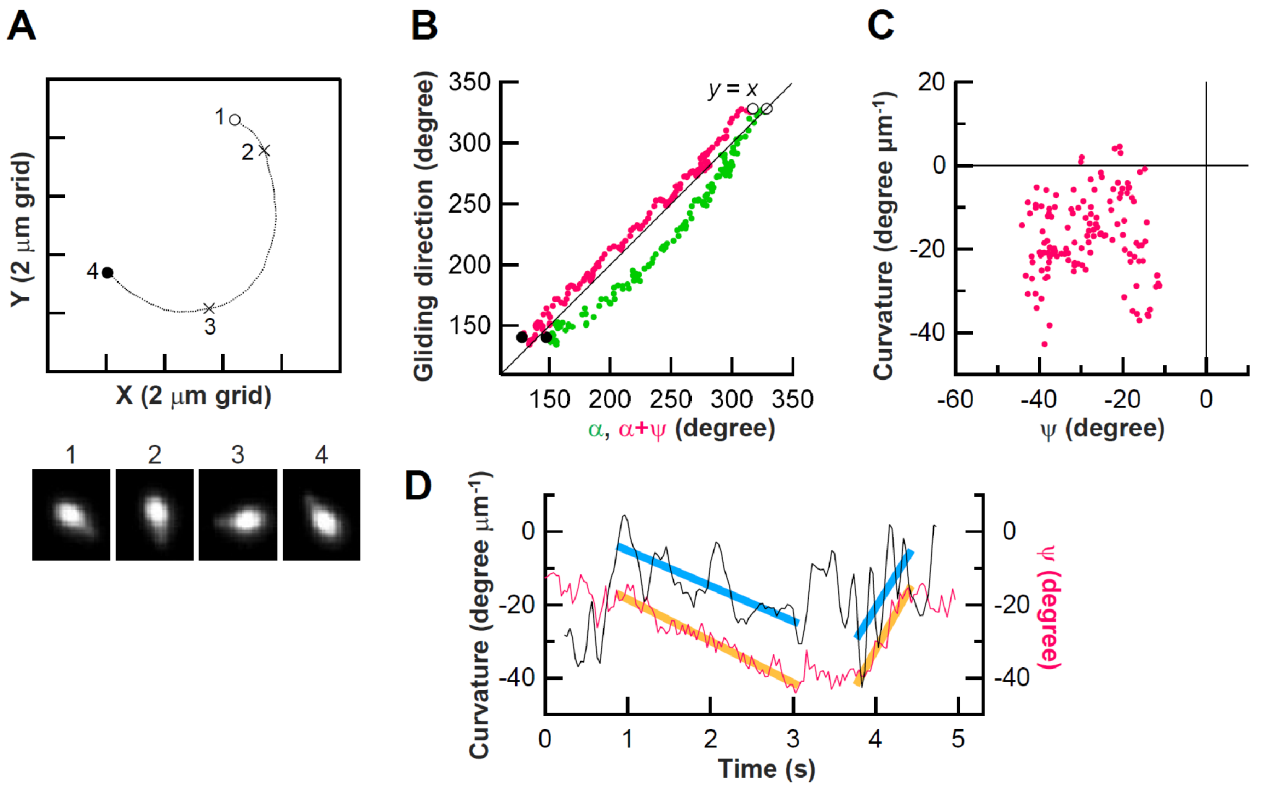


**Figure 2** A typical example of data analysis. (A) *Top*, example of trajectories of gliding *M. mobile* cell traced 30 frames per second for 5 s. Open and filled circles represent the start and end points, respectively. *Bottom*, snapshots of dark-field image of the cell at points indicated by numbers in the trajectory. Square size, 3.0×3.5 μm$^2$. (B) *Green*, relationship between the body angle against *XY*-plane, α, and gliding direction. *Magenta*, relationship between the head angle against *XY*-plane, α+ψ, and gliding direction. Both plots are taken from one dataset of sequential images and their trajectory represented in A. Degree 0 is defined as the plus direction of *X*-axis. (C) Relationship between ψ and the curvature of the gliding in A. (D) Timecourse of ψ (magenta) and the curvature (black). Cyan lines display the range where ψ and the curvature decreased and increased in sync.

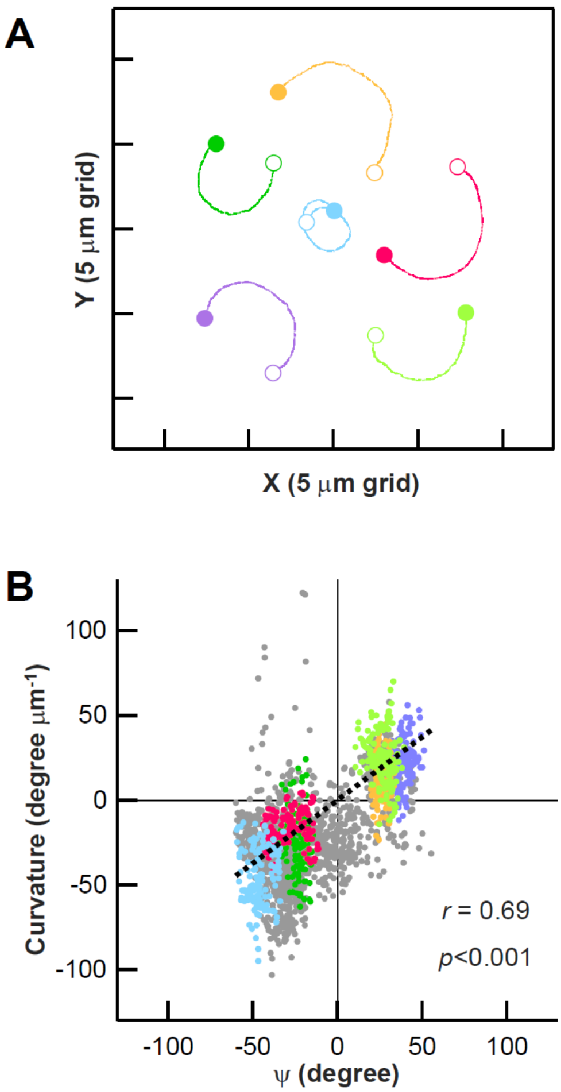


**Figure 3** (A) Example of trajectories of gliding *M. mobile* cells traced 30 frames per second for 5 s. Open and filled circles represent the start and end points, respectively, in each trajectory. (B) Relationship between a head angle against a cell body, ψ, and trajectory curvature. Angles of clockwise and counterclockwise are indicated by – and +, respectively. Each point represents a single videoframe (*X*-axis) and a curvature estimated from a trajectory of ±5 frames of the videoframe (*Y*-axis). Magenta, light blue, green, light green, orange and purple dots represent measurements from individual cells whose trajectories are shown in A. Forty-seven cells were analyzed in total, but our procedure worked properly only for 16 cells to fit all sequential images for each 5 s run. The plot includes ~2100 points of 16 cells, and the grey are data from 10 cells.

to determine its center [24]. We previously applied this method to track dark-field images of *M. mobile* with single Gaussian function having large and small deviations in the long and short axes, respectively [22]. In this study, we extended this approach further: a single fitting function involving double 2D Gaussians (one Gaussian for the cell body and the other for the head; see *Materials and Methods*) was applied to a raw image. As shown in Figure 1B, the raw image (*left*) and the reconstructed image by double Gaussians (*right*) were identical, showing that our fitting method worked well enough to describe the cell shape.

The advantage of this method is that we quantitatively evaluated the angle of the head portion against the body. In Figure 1C, fitting for the body (green) and head (magenta) is separately viewed with final fitting parameters. The head was tilted 30.2° rightward in this example, which was defined as the difference between the long axes of the two Gaussians (Figure 1C *schematic*). The image profiles along an axis were almost identical (*left* in Figure 1C) between the raw image (black) and the fitted image (cyan), showing that the fitting function we applied worked properly (see *Materials and Methods* for the function in detail). In this example, the parameter corresponding to the eccentricity of two Gaussian centers, *R*, was 1.76. The fitting procedure did not work well when $R<1.0$ in our image of cells, because peaks of two Gaussian functions became closer and each distribution highly overlapped. Other examples demonstrate that double Gaussians successfully reconstructed cell shapes with a nearly straight head (Figure 1D, 7.2° rightward, $R = 1.86$) and an inversely tilted head (Figure 1E, 38.8° leftward, $R = 1.64$). The range of ψ was restricted ±60° in our fitting to reconstruct curved configuration of each cell.

**Bacterial shape correlates with gliding trajectory**

To explore the origin of a particular trajectory of gliding *M. mobile*, we focused on not a straight but curved trajectory (Figure 2A *Top*). As previously reported, the direction of the protrusion of the cell roughly coincides with the gliding direction (Figure 2A *Bottom*). We found that the long axis of the ellipsoidal body, α, was correlated but not simply proportional to the gliding direction (Figure 2B green). Rather, the head axis against *XY*-plane, α+ψ, is clearly proportional to the gliding with the slope of 1 (Figure 2B magenta). This suggests that the axis of the body is not a sole determining factor and the head mainly leads the direction of displacement. Additionally, magenta plots in Figure 2B slightly shifted upward from '$y = x$ line', but green plot shifted downward. These opposite gaps imply that the body part also affects the gliding direction as the angle offset to guide the velocity vector. We infer that the power produced by gliding units, which localize around the neck (Figure 1A), directly couples to the head that works as a rudder, and the body could work as the drag to set the final gliding angle at each moment.

To check whether the head critically guides the gliding direction, ψ was compared to the curvature of the gliding. Our idea is that the curvature should increase and decrease when the ψ becomes large and small, respectively, if the head literally works as the rudder for single-bacterium gliding. For calculation, the curvature was concisely determined as a

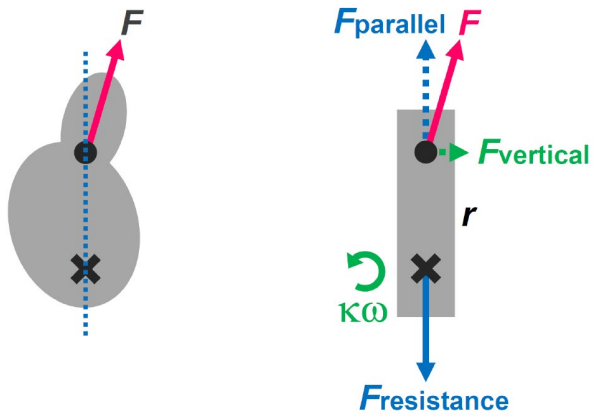


**Figure 4** Model for the mechanism of how cell shape correlates to the curved trajectory. *Left*, the angle of the head is slightly tilted to the right against the cell body. Dot and magenta arrow represent the localization of gliding machinery and its force vector, respectively, whereas the cross is the assumed point that adheres to the substrate with non-specific binding. *Right*, the simplified diagram on the *left*. In this diagram, simplified cell (gray) as a rod shape, and forces and torque imposed upon the rod. Arrows with the same color (blue and green) are balanced. See text for more details.

quotient of angle change of the displacement vector divided by the speed of the cell center. As shown in *Y*-axis in Figure 2C, curvature was distributed largely, because the center of the cell wiggled during displacement in the magnified view and thus the estimated angle fluctuates. ψ also distributed largely (*X*-axis in Figure 2C), which may imply a rolling of the cell. The change in apparent angle between a head and a body could occur in the projection to *XY*-plane when an asymmetric and bent object rolls. Still, correlation between curvature and ψ was barely distinguished in part in the timecourse of two parameters (cyan and orange lines in Figure 2D) but not stable in all points. To confirm the correlation between ψ and the curvature, we performed the same analysis in multiple cells ($n$ = 16). There were examples in Figure 3A that showed counterclockwise (CCW; orange, light green and purple) and clockwise (CW; green, light blue and magenta) circular trajectories. The representative movie, which includes the analyzed gliding cell (purple in Figure 3A), is shown in Supplementary Movie S1. Notably, CCW and CW trajectories locate in the first and third quadrants, respectively, in most plots, suggesting the above correlation strongly (Figure 3B). Data points were fitted well in a linear manner with a restriction passing the origin (dashed line in Figure 3B; the $r$-value = 0.69 and $p < 0.001$). Additionally, 67% of datapoints located in the third and fourth quadrants. This asymmetry indicates that the curve direction is biased to clockwise, which coincides with the previous report [8] taking account of the microscope difference between upright and inverted ones.

In previous contribution regarding *Mycoplasma genitalium*, Burgos et al. suggested similar conclusion with us, i.e., the correlation of the trajectory and cell shapes [34], although none of the motility structure is homologous between two species, *M. mobile* and *M. genitalium*. They observed the modification of both terminal organelle curvature under an electron microscope by deleting specific gene, and the deletion also modifies gliding curvature as a population. Note that we here successfully quantified the cell structure under an optical microscope (cf. Figure 1 B-E) without using any electron microscope, which enable to visualize true gliding behavior of each cell at the single-cell level.

We also found the head tends to bend rightward, watching cells that glided on the bottom surface from the top: 62% of datapoints located in second and third quadrants in Figure 3B. This observation raises an apparent paradox, because generally speaking, bacteria do not have the asymmetry between a ventral side and a dorsal side, and so right-left asymmetry could not be defined. However, in case that the rolling motion of the cell around the gliding axis in right-handed corkscrewing manner occurs at the moment when the cell adheres to the substrate, rightward asymmetric bending may appear as the bent head would asymmetrically hinder the rolling and terminate the corkscrewing. Asymmetric pulling of legs connecting to motors was previously suggested [8], and this asymmetrical could contribute to the rolling motion. Other explanations, such as possible asymmetries in all three axes (front-rear, ventral-dorsal and right-left) of the head-body junction of *M. mobile*, may be attributable to rightward head-bending of gliding cells. This point will be addressed with more detailed measurements in both optical and electron microscopes in near future.

**Model**

The simple explanation for our findings shown in Figure 2B and 3B is that there was a single (or more) point(s) in the cell body that attached to the substrate during gliding, possibly accompanying non-specific binding. In the *left* schematic in Figure 4, a dot and a cross represent the location of gliding machinery and the non-specific attachment point, respectively. A magenta arrow $F$ is the sum of force vectors produced by multiple motor units, ~100 at the bottom side [12]. Note that the cell should show a straight trajectory along the arrow $F$ if there are no additional attachment points such as the cross. In the *right* schematic, the cell body is simplified as a rod to intuitively understand the balance of multiple forces. $\boldsymbol{F}$ imposed on the dot is decomposed to $\boldsymbol{F}_{\mathrm{parallel}}$ and $\boldsymbol{F}_{\mathrm{vertical}}$, and $\boldsymbol{F}_{\mathrm{parallel}}$ is equal to $-\boldsymbol{F}_{\mathrm{resistance}}$ imposed at the cross (note that linear acceleration is generated in case that $\boldsymbol{F}_{\mathrm{resistance}}$ is not equal to $\boldsymbol{F}_{\mathrm{parallel}}$, so these two forces should be always balanced in the timescale of our measurement). We assumed that $F_{\mathrm{resistance}}$ worked as drag that increases with gliding velocity; this concept is generally accepted and crucially determines the final speed driven by molecular motors as the balance between motor force and drag [11]. The key of our model is that there are drags at the cross not only in a

linear direction but also in a rotational direction. Morio et al. also mentioned the drag as the cause of the stable curved trajectory, but geometrical point of view was lack in their argument [8]. In contrast, our formulation designates the rotational drag (green arrow), which increased as angular speed (ω) increased and thus could be assigned as κω as the simplest approximation, where κ is the drag coefficient for rotation. In other words, we put the localization of the drag (cross) *r* apart from the center of the summed force-vector (dot), which allows to generate a torque enough to explain a curved trajectory. To keep a constant curvature when the cell glides, κω was balanced to the torque at the dot, $r \times F_{\mathrm{vertical}}$. As a consequence, ω, which directly correlates to the curvature of the trajectory, is determined by $F_{\mathrm{vertical}}$. Because the amplitude of $F_{\mathrm{vertical}}$ is the cosine of $\boldsymbol{F}$ and thus is determined by the tilting of the head, the direction of the head guides the gliding curvature in our observations. The above framework explains a curved trajectory of gliding bacteria at the single-cell level. To the best of our knowledge, our simple explanation is the first model that links the asymmetric configuration of a bacterial cell directly to its gliding motility. The heterogeneity of the arrangement of multiple motors was previously suggested as an interpretation [8], which we conclude to be insufficient as discussed above. By extending our new model with a more precise formulation that involves multiple motors and adhering points, other curved trajectories of gliding bacteria [6] or motor proteins [35] may be described in detail in the near future.

## Conclusion

We developed the method to fit the intensity profile of single-bacterium image under optical microscopy, which allows us to analyze the shape of its cell body quantitatively. The correlation between gliding direction and cell configuration was suggested in case of *M. mobile*. Furthermore, we hypothesize the model for the mechanism to explain the correlation, which could be extended to circular trajectories induced by biomolecules.

## Conflict of Interest

We declare no competing financial interests.

## Author Contributions

Kana Suzuki: Writing – original draft, Data curation, Formal analysis. Daisuke Nakane: Writing – review & editing, Conceptualization. Masaki Mizutani: Writing – review & editing. Takayuki Nishizaka: Writing – review & editing, Supervision.

## Data Availability

The evidence data generated and/or analyzed during the current study are available from the corresponding author on reasonable request.

## Acknowledgements

This study was supported in part by the Japan Society for the Promotion of Science KAKENHI [grants JP22H05066 (to D.N.) and JP22H02589 (to T.N.)].

## References

[1] Miyata, M., Robinson, R. C., Uyeda, T. Q. P., Fukumori, Y., Fukushima, S., Haruta, S., et al. Tree of motility - A proposed history of motility systems in the tree of life. Genes Cells 25, 6-21 (2020). https://doi.org/10.1111/gtc.12737

[2] Berg, H.C. Random Walks in Biology (Princeton University Press, Princeton, 1984).

[3] Cohen, E.J., Nakane, D., Kabata, Y., Hendrixson, D. R., Nishizaka, T., Beeby, M. *Campylobacter jejuni* motility integrates specialized cell shape, flagellar filament, and motor, to coordinate action of its opposed flagella. PLoS Pathog. 16, e1008620 (2020). https://doi.org/10.1371/journal.ppat.1008620

[4] Nakane, D., Ito, T., Nishizaka, T. Coexistence of two chiral helices produces kink translation in *Spiroplasma* swimming. J. Bacteriol. 202, 00735-19 (2020). https://doi.org/10.1128/JB.00735-19

[5] Nakane, D., Nishizaka, T. Asymmetric distribution of type IV pili triggered by directional light in unicellular cyanobacteria. Proc. Natl. Acad. Sci. U.S.A. 114, 6593-6598 (2017). https://doi.org/10.1073/pnas.1702395114

[6] Nakane, D., Odaka, S., Suzuki, K., Nishizaka, T. Large-scale vortices with dynamic rotation emerged from monolayer collective motion of gliding *Flavobacteria*. J. Bacteriol. 203, e0007321 (2021).

https://doi.org/10.1128/JB.00073-21
[7] Nakane, D., Sato, K., Wada, H., McBride, M. J., Nakayama, K. Helical flow of surface protein required for bacterial gliding motility. Proc. Natl. Acad. Sci. U.S.A. 110, 11145-11150 (2013). https://doi.org/10.1073/pnas.1219753110
[8] Morio, H., Kasai, T., Miyata, M. Gliding direction of *Mycoplasma mobile*. J. Bacteriol. 198, 283-290 (2016). https://doi.org/10.1128/JB.00499-15
[9] Nakane, D., Kabata, Y., Nishizaka, T. Cell shape controls rheotaxis in small parasitic bacteria. PLoS Pathog. 18, e1010648 (2022). https://doi.org/10.1371/journal.ppat.1010648
[10] Purcell, E. M. Life at low Reynolds number. Am. J. Phys. 45, 3-11 (1977).
[11] Tawada, K., Sekimoto, K. A physical model of ATP-induced actin-myosin movement in vitro. Biophys. J. 59, 343-356 (1991). https://doi.org/10.1016/S0006-3495(91)82228-7
[12] Miyata, M. Unique centipede mechanism of *Mycoplasma* gliding. Annu. Rev. Microbiol. 64, 519-537 (2010). https://doi.org/10.1146/annurev.micro.112408.134116
[13] Rosengarten, R., Kirchhoff, H. Gliding motility of *Mycoplasma* sp. nov. strain 163K. J. Bacteriol. 169, 1891-1898 (1987). https://doi.org/10.1128/jb.169.5.1891-1898.1987
[14] Jaffe, J. D., Stange-Thomann, N., Smith, C., DeCaprio, D., Fisher, S., Butler J., et al. The complete genome and proteome of *Mycoplasma mobile*. Genome Res. 14, 1447-1461 (2004). https://doi.org/10.1101/gr.2674004
[15] Uenoyama, A., Miyata, M. Identification of a 123-kilodalton protein (Gli123) involved in machinery for gliding motility of *Mycoplasma mobile*. J. Bacteriol. 187, 5578-5584 (2005). https://doi.org/10.1128/JB.187.16.5578-5584.2005
[16] Seto, S., Uenoyama, A., Miyata, M. Identification of a 521-kilodalton protein (Gli521) involved in force generation or force transmission for *Mycoplasma mobile* gliding. J. Bacteriol. 187, 3502-3510 (2005). https://doi.org/10.1128/JB.187.10.3502-3510.2005
[17] Uenoyama, A., Kusumoto, A., Miyata, M. Identification of a 349-kilodalton protein (Gli349) responsible for cytadherence and glass binding during gliding of *Mycoplasma mobile*. J. Bacteriol. 186, 1537-1545 (2004). https://doi.org/10.1128/JB.186.5.1537-1545.2004
[18] Toyonaga, T., Kato, T., Kawamoto, A., Kodera, N., Hamaguchi, T., Tahara, Y., et al. Chained structure of dimeric $F_1$-like ATPase in *Mycoplasma mobile* gliding machinery. mBio 12, e0141421 (2021). https://doi.org/10.1128/mBio.01414-21
[19] Tulum, I., Kimura, K., Miyata, M. Identification and sequence analyses of the gliding machinery proteins from *Mycoplasma mobile*. Sci. Rep. 10, 3792 (2020). https://doi.org/10.1038/s41598-020-60535-z
[20] Miyata, M., Hamaguchi, T. Prospects for the gliding mechanism of *Mycoplasma mobile*. Curr. Opin Microbiol. 29, 15-21 (2016). https://doi.org/10.1016/j.mib.2015.08.010
[21] Tulum, I., Yabe, M., Uenoyama, A., Miyata, M. Localization of P42 and $F_1$-ATPase α-subunit homolog of the gliding machinery in *Mycoplasma mobile* revealed by newly developed gene manipulation and fluorescent protein tagging. J. Bacteriol. 196, 1815-1824 (2014). https://doi.org/10.1128/JB.01418-13
[22] Kinosita, Y., Nakane, D., Sugawa, M., Masaike, T., Mizutani, K., Miyata, M., et al. Unitary step of gliding machinery in *Mycoplasma mobile*. Proc. Natl. Acad. Sci. U.S.A. 111, 8601-8606 (2014). https://doi.org/10.1073/pnas.1310355111
[23] Nakane, D., Miyata, M. Cytoskeletal "jellyfish" structure of *Mycoplasma mobile*. Proc. Natl. Acad. Sci. U.S.A. 104, 19518-19523 (2007). https://doi.org/10.1073/pnas.0704280104
[24] Thompson, R.E., Larson, D.R., Webb, W.W. Precise nanometer localization analysis for individual fluorescent probes. Biophys. J. 82, 2775-2783 (2002). https://doi.org/10.1016/S0006-3495(02)75618-X
[25] Fujimura, S., Ito, Y., Ikeguchi, M., Adachi, K., Yajima, J., Nishizaka, T. Dissection of the angle of single fluorophore attached to the nucleotide in corkscrewing microtubules. Biochem. Biophys. Res. Commun. 485, 614-620 (2017). https://doi.org/10.1016/j.bbrc.2017.01.165
[26] Hasimoto, Y., Sugawa, M., Nishiguchi, Y., Aeba, F., Tagawa, A., Suga, K., et al. Direct identification of the rotary angle of ATP cleavage in $F_1$-ATPase from Bacillus PS3. Biophys. J. 122, 554-564 (2023). https://doi.org/10.1016/j.bpj.2022.12.027
[27] Masaike, T., Koyama-Horibe, F., Oiwa, K., Yoshida, M., Nishizaka, T. Cooperative three-step motions in catalytic subunits of $F_1$-ATPase correlate with 80 degrees and 40 degrees substep rotations. Nat. Struct Mol. Biol. 15, 1326-1333 (2008). https://doi.org/10.1038/nsmb.1510
[28] Sugawa, M., Okada, K. A., Masaike, T., Nishizaka, T. A change in the radius of rotation of $F_1$-ATPase indicates a tilting motion of the central shaft. Biophys. J. 101, 2201-2206 (2011). https://doi.org/10.1016/j.bpj.2011.09.016
[29] Yajima, J., Mizutani, K., Nishizaka, T. A torque component present in mitotic kinesin Eg5 revealed by three-dimensional tracking. Nat. Struct Mol. Biol. 15, 1119-1121 (2008). https://doi.org/10.1038/nsmb.1491
[30] Uenoyama, A., Miyata, M. Gliding ghosts of *Mycoplasma mobile*. Proc. Natl. Acad. Sci. U.S.A. 102, 12754-12758

(2005). https://doi.org/10.1073/pnas.0506114102
[31] Uenoyama, A., Seto, S., Nakane, D., Miyata, M. Regions on Gli349 and Gli521 protein molecules directly involved in movements of *Mycoplasma mobile* gliding machinery, suggested by use of inhibitory antibodies and mutants. J. Bacteriol. 191, 1982-1985 (2009). https://doi.org/10.1128/JB.01012-08
[32] Ayano, M., Sawamura, Y., Hongo-Hirasaki, T., Nishizaka, T. Direct visualization of virus removal process in hollow fiber membrane using an optical microscope. Sci. Rep. 11, 1095 (2021). https://doi.org/10.1038/s41598-020-78637-z
[33] Kirchhoff, H., Rosengarten, R. Isolation of a motile mycoplasma from fish. J. Gen. Microbiol. 130, 2439-2445 (1984). https://doi.org/10.1099/00221287-130-9-2439
[34] Burgos, R., Pich, O. Q., Querol, E., Pinol, J. Deletion of the *Mycoplasma genitalium* MG_217 gene modifies cell gliding behaviour by altering terminal organelle curvature. Mol. Microbiol. 69, 1029-1040 (2008). https://doi.org/10.1111/j.1365-2958.2008.06343.x
[35] Lebreton, G., Géminard, C., Lapraz, F., Pyrpassopoulos, S., Cerezo, D., Spéder, P., et al. Molecular to organismal chirality is induced by the conserved myosin 1D. Science 362, 949-952 (2018). https://doi.org/10.1126/science.aat8642